Channeling radiation of electrons in natural diamond crystals and their coherence and occupation lengths

H. Genz, L. Groening, P. Hoffmann-Stascheck, and A. Richter
Institut für Kernphysik, Technische Hochschule Darmstadt, D-64289 Darmstadt, Germany

M. Höfer and J. Hormes
Physikalisches Institut, Universität Bonn, D-53115 Bonn, Germany

U. Nething
Forschungszentrum Rossendorf e.V., D-01314 Dresden, Germany

J. P. F. Sellschop
University of the Witwatersrand, 2050 Johannesburg, South Africa

C. Toepffer and M. Weber
Institut für Theoretische Physik, Universität Erlangen, D-91058 Erlangen, Germany
(Received 24 August 1995)

Measurements have been performed at the superconducting Darmstadt electron linear accelerator (S-DALINAC) to investigate systematically channeling radiation produced by bombarding natural diamond crystals with thicknesses of 13, 20, 30, and 55 μm with electrons at 5.2 and 9.0 MeV. Planar channeling from the (110) and (111) planes was studied for a variety of transitions with respect to their energy, intensity, and linewidth. Axial channeling from the $\langle 110 \rangle$ axis could be detected as well. It was found that the intensity increases as a function of the crystal thickness, and values up to 7.7×10^{-2} photons/$e$sr could be obtained, which is the highest intensity at low electron energies achieved so far. The intensity increases with electron energy as $\gamma^{5/2}$. The $1/e$ occupation length deduced from the photon yield as a function of the crystal thickness was found to be $l_{\mathrm{occ}} \approx 29$ and 85 μm for planar and for axial channeling, respectively. These values are by far the largest ever observed. Comparison with a quantum mechanical theory of channeling radiation exhibits fairly good agreement for the intensity and linewidth provided that contributions caused by electronic scattering and Bloch wave broadening, which actually are largest for diamond, are properly taken into account. It turns out that multiple scattering dominates in the planar case and single scattering for the axial channeling. The coherence length could be deduced to be of the order of 0.7 μm, which is about a factor of 2 larger than observed before in silicon.

I. INTRODUCTION

Channeling radiation is emitted by relativistic electrons passing through single crystals along a direction of high symmetry, a plane or an axis. The radiation is forward directed into a narrow cone with an angle of emission $\Theta \sim \gamma^{-1}$ and many of its outstanding features have been the subject of numerous experimental and theoretical investigations.[1–20] There are several interesting and potentially very useful characteristics of channeling radiation: It is energetic, bright, and tunable and it is of narrow linewidth in the spectral peaks. Also, because channeling radiation has the same time structure as the incident electron beam, the pulse of radiation can be of extremely short duration, e.g., 2 ps,[15,18,21] while being furnished continuously at the same time. All these qualities make channeling radiation a unique photon source in the x-ray region,[19] for which there is a vast demand,[22] especially if this can be achieved with accelerators much smaller and less expensive than storage rings or synchrotrons.

Since the characteristic features of the channeling radiation spectrum depend strongly on the crystal and its properties, the optimum source crystal has to be searched for. For possible applications, an intense source delivering of the order of 10^{12} photons/s with a narrow bandwidth of about 10% full width at half maximum (FWHM), which is collimated and tunable between about 10 and 40 keV, is required. Since the crystal will also have to stand high electron beam currents of several hundred mA, it has to have a high thermal conductivity.

Regarding these prerequisites, diamond appears to be a strong candidate for the production of intense, quasimonochromatic x rays using channeling.[10,12,15,17,23–25] Diamond shows not only a spectrum with very narrow lines but it meets also most of the criteria asked for. Due to its large thermal conductivity and exceptionally high Debye temperature, diamonds can withstand intense electron beam currents and yield the largest intensities observed so far. Furthermore, since the new generation of electron accelerators provide electron beams of extremely low divergence,[23,25–29] a maximum population probability of channeling states can be achieved also at full beam current. It thus appears likely that the intensity obtained so far (i.e., 2×10^{10} photons/s) can be extended to the required limit quoted above.

Since for application as an intense photon source detailed knowledge on the observables radiation energy, line intensity, and linewidth and the angular distribution of the radiation are of crucial importance, we have concentrated in the present work on a systematical investigation of these quantities and a comparison with a quantum mechanical theory, which is based on an extended perturbative approach. While the energy of the transitions observed in channeling is in general in good agreement with the calculation for the quantized states in the crystal potential, not much is known about the two other quantities. Regarding the $1/e$ occupation length l_{occ}, which determines the length the electron stays in its state, Gary *et al.*[24] predicted for 30 MeV electrons in diamond a value of 80 μm using a scaling procedure proposed by Andersen. The coherence of the state on the other side is described by the length the electron stays in its specific state without change of phase. This quantity is directly related to the linewidth. Investigations performed by Klein *et al.*[15] at electron energies between 17 and 54 MeV exhibited, however, that the observed linewidth exceeds the theoretical prediction by a factor of 2. This discrepancy was believed to be caused by incoherent scattering at crystal defects. Since, however, also other effects, like, e.g., the electron beam divergence affecting the linewidth due to Bloch wave broadening, can be of importance as well, it is necessary to investigate these phenomena in more detail.

It is the aim of this paper to elucidate how the linewidth and line intensity depend on bombarding energy, crystal thickness, the planes, and the axes. From these findings the observable coherence and occupation length will be derived and attention will be paid to the equilibrium population of states in diamond. A small part of this work has been published before,[20] where the intensity was compared with the results obtained from an approximative solution of a master equation that governs the feeding and depopulation of the states in the crystal potential. In the present paper the entire bulk of data will be presented and compared to calculations based on an extended theoretical treatment of the observables, which will be explained in Sec. II. Thermal and valence electron scattering as well as core electron scattering will be included both for the calculation of the linewidth and the population redistribution. The electronic part of the linewidth is found not to be negligible. Contributions to the linewidth due to Bloch wave broadening are considered as well. It can be easily incorporated with the knowledge of the band dispersion, calculated by the so-called many-beam method. More effort must be taken to include the contribution of the Doppler broadening, which arises from the growth of the beam divergence with increasing penetration depth of the electrons in the crystal. This quantity has often been estimated from the corresponding value in an amorphous target. We calculate it by a method which takes into account the modified scattering probabilities under channeling conditions.[30]

In Sec. III the experimental setup, operating conditions, and the data accumulation and reduction procedures are described briefly. The results are presented in Sec. IV, which is followed by a discussion and comparison with theory. The paper closes with conclusions in Sec. V.

II. THEORY OF CHANNELING

A. Quantum mechanical description of planar channeling

For relativistic electrons moving under a small angle ψ less than the critical Lindhard angle ψ_c to a crystal plane planar channeling takes place.[31] According to Lindhard, as a first approximation the crystal potential is averaged over the plane of incidence. Furthermore, an average over thermal vibrations is performed.

Due to the nonrelativistic character of the motion in the direction transversal to the channeling plane and the translational invariance of the Lindhard continuum potential along the plane, the solution of the Dirac equation separates into a plane wave with wave vector $p_z/\hbar$ in the longitudinal direction and a transverse wave function $\phi(x)$, which is approximated by the solution of a Schrödinger like equation with a relativistic mass $m\gamma$,

$$\left(\frac{\hat{p}_x^2}{2m\gamma}+\hat{V}(x)\right)\phi(x)=\epsilon\phi(x) \quad \text{where} \quad \gamma=(1-\beta^2)^{-1/2}. \tag{1}$$

The total energy E of the electron is related to the transverse energy eigenvalue ϵ by $E\approx\epsilon+\sqrt{(cp_z)^2+(mc^2)^2}$. Since $V(x)$ represents the periodic Lindhard continuum potential, its solutions are Bloch waves,

$$\phi_{n,\kappa}(x)=\langle x|n,\kappa\rangle=\frac{1}{\sqrt{L_x}}e^{i\kappa x}u_{n,\kappa}(x), \tag{2}$$

with Bloch momentum κ. Here L_x is the length of the normalization box and the periodic part of the Bloch wave, $u_{n,\kappa}(x)$, satisfies $u_{n,\kappa}(x)=u_{n,\kappa}(x+d)$ with d being the interplanar distance.

Channeling states, described in this simple picture, undergo a number of perturbations, some of which are discussed in the following. First, channeling radiation itself will be described in the following section as radiative transitions between unperturbed states. However, for its detailed properties, like intensity and linewidth, also the interactions with thermal vibrations and crystal electrons have to be included. These methods will be quickly reviewed in Sec. II C.

B. Intensity of channeling radiation

Coupling to the electromagnetic field induces radiative transitions between transverse states $|i,\kappa\rangle$ and $|f,\kappa\rangle$. Using perturbation theory one finds, for the differential transition probability for channeling radiation per crystal length dz, frequency interval $d\omega$, and angle element $d\Omega$,

$$\frac{d^3W_{fi}}{dz\,d\Omega\,d\omega}=\frac{e^2}{\pi(mc^2)^2}\frac{\hbar\omega}{2\gamma^2(1-\beta\cos\vartheta)}|\langle f,\kappa|p_x/\hbar|i,\kappa\rangle|^2\delta \times\left(\omega-\frac{\omega_{if}}{1-\beta\cos\vartheta}\right) \times\left(\sin^2\varphi+\cos^2\varphi\frac{(\beta-\cos\vartheta)^2}{(1-\beta\cos\vartheta)^2}\right), \tag{3}$$

which is summed over both directions of polarizations.[32,33] Here an infinite lifetime of the initial and final states was assumed, resulting in a δ-shaped line. The angles ϑ and φ are polar and azimuthal angles measured from the z and x axes, respectively.

As can be seen from the last equation, the energy of the photon emitted in the direction of the channeled electron ($\vartheta=0$) exceeds the transverse energy difference $\hbar\omega_{if}$ by a factor $2\gamma^2$ due to the relativistic Doppler effect and is maximum in this direction as well as the emitted intensity. In this case the last angle-dependent term in Eq. (3) simplifies to unity.

C. Transition probabilities and linewidths

Also a number of perturbations exists leading to nonradiative transitions between channeling states and thus limiting their lifetime. This results both in a nonzero linewidth of the emitted radiation and in a redistribution of the initial population of channeling states.

1. Thermal scattering

As a rough but nevertheless often satisfactory approximation the periodic crystal potential can be built up by a superposition of atomic potentials $V_a(\vec{r})$ located at each lattice site of the crystal. An additional approximation concerns the thermal vibrations. In the continuum potential thermal deformations are included only on their average. For the calculation of energy levels this is a sufficient approximation. However, the deviation of the thermally deformed crystal potential $\Sigma V_a(\vec{r}-\vec{r}_i)$ of the N_a crystal atoms from the thermally averaged continuum potential $V(x)$,

$$V_{\rm th}(\vec{r}_1,\ldots,\vec{r}_{N_a},\vec{r})=\sum_{i=1}^{N_a} V_a(\vec{r}-\vec{r}_i)-V(x), \tag{4}$$

leads to transitions between unperturbed channeling states, i.e., the solutions of Eq. (1). The differential transition probability resulting from Fermi's golden rule averaged over all thermal displacements $\vec{r}_1,\ldots,\vec{r}_{N_a}$ is given by Refs. 32,34 as

$$\left\langle \frac{d^3W_{fi}^{\rm th}}{dz\,d\kappa\,dk_y}\right\rangle_{r_1,\ldots,r_{N_a}} = \frac{n_a}{(2\pi\hbar c)^2}\left[\left\langle\left|\langle f,\kappa_f|V_{q,a}(x-x_0)L_x|i,\kappa_i\rangle_\infty\right|^2\right\rangle - e^{-q^2u^2}\left|\langle f,\kappa_f|\langle V_{q,a}(x-x_0)\rangle_{x_0}L_x|i,\kappa_i\rangle_\infty\right|^2\right], \tag{5}$$

where the angular brackets $\langle\cdots\rangle_{x_0}$ denote the average over all thermal displacements from a lattice site, which is indicated by indices at the angular brackets. For the probability distribution of the latter a product of independent Gaussians with a mean square amplitude u^2 for each atom was assumed. In Eq. (5), $q=k_y^f-k_y^i$ is the y momentum transfer, n_a the atomic density, and $V_{q,a}(x)=\int dz\,dy\,e^{-iqy}V_a(r)$. The index ∞ at the inner product indicates that the integration is extended from the normalization box to the interval $[-\infty,+\infty]$. This approximation is justified since the inner product now contains the transformed atomic potential $V_{q,a}(x)$, which drops off far from the atom, instead of the periodic continuum potential $V(x)$. (Note that the transition probability [Eq. (5)] is effectively independent of L_x, although explicitly apparent in Eq. (5), since the extra L_x cancels the normalization factor in the wave function, Eq. (2).)

2. Inelastic electronic scattering

Excitation of the N_e crystal electrons is described by the Coulomb interaction with the channeling electrons,

$$V_e(R_1,\ldots,R_{N_e},r)=\sum_{i=1}^{N_e}\frac{e^2}{|R_i-r|}, \tag{6}$$

and two cases must be distinguished:

Valence electron scattering is best approximated[32] as scattering of the incident electron at a free electron gas of homogeneous density $n_v=Z_v n_a$, where Z_v denotes the number of valence electrons per atom. As a simple model for the spectrum of the target electrons, excitations are considered to consist only of plasmon excitation (plasma frequency ω_p) for low momentum transfer q and excitation of a single electron with energy $\hbar^2q^2/(2m)$ for higher q. As shown in Ref. 32, these assumptions yield

$$\frac{d^3W_{fi}^{\rm val}}{dz\,d\kappa\,dk_y}=Z_v n_a\left(\frac{2e^2}{\hbar c}\right)^2\sum_{q_x}\frac{\left|\langle i\kappa_i|e^{-iq_xx}|f\kappa_f\rangle\right|^2}{\left[q^2+\left(\frac{\omega_p}{c}\right)^2\right][q^2+q_0^2]} \tag{7}$$

for the differential transition probability due to valence electron scattering with a Bloch momentum transfer κ and a y momentum transfer k_y. Here q_0 has been defined via $(\hbar^2/2m)q_0^2=\hbar\omega_p$. Furthermore, $q^2=q_x^2+k_y^2$ holds by momentum conservation in the y direction. The sum over q_x runs over all integer multiples of $2\pi/L_x$, since a box normalization with a normalization length L_x was used in Eq. (2) for the channeling wave function.

In the case of *core electron* scattering[35] the energy spectrum of the crystal electrons is neglected completely. In contrast to the case of valence electrons the density of the core electrons can be included exactly via the Fourier transform $\tilde{\rho}(q_x,q_y)=\int d^3r|\varphi_{\rm core}|^2e^{-i(q_xx+q_yy)}$ of the density. For the transition probability this results in

$$\left\langle \frac{d^3W_{fi}^{\rm core}}{dz\,d\kappa\,dk_y} \right\rangle_{r_1,\ldots,r_{N_c}} = Z_c n_a \left(\frac{2e^2}{\hbar c}\right)^2 \sum_{q_x} \sum_{q_x'} \frac{\langle i\kappa_i | e^{iq_x x} | f\kappa_f \rangle}{q^2} \frac{\langle f\kappa_f | e^{-iq_x' x} | i\kappa_i \rangle}{q'^2} e^{-\frac{1}{2}u^2(q_x-q_x')^2} [\tilde{\rho}(q_x-q_x',0) - \tilde{\rho}(q_x,k_y)\tilde{\rho}(-q_x',-k_y)]. \quad (8)$$

By summation of (5), (7), and (8) over all final states the total transition probability W_n of a state n into any other state can be obtained.[32,35] The quantity W_n is related to the width w_n of the state as $w_n = \hbar c W_n$.

The width Γ_{fi} of a radiative transition from a state i to a state f observed in the laboratory frame can be approximated as the sum of the width W_i and W_f multiplied by the Doppler factor $2\gamma^2$, yielding

$$\Gamma_{fi} = \Gamma_i + \Gamma_f = 2\gamma^2 (W_i + W_f). \quad (9)$$

In the present work, however, the incoherent width Γ_{fi} was calculated according to Ref. 32 including a small correction from intraband scattering, which modifies the more simple approximation (9) (see Ref. 32 for details).

D. Further mechanisms of line broadening

In addition to limiting the lifetime of the channeling states, the above-mentioned scattering mechanisms also lead to an indirect line broadening by increasing the beam divergence in the y direction. Due to this divergence, photons emitted from the channeled electron reach the detector under a nonzero angle to the direction of the electron. Equation (3) shows that under these circumstances the relativistic Doppler effect reduces the energy of the emitted photon.

Furthermore, the band dispersion of energy levels relevant for the channeling radiation may give an important contribution to the linewidth for not too deeply bound initial and final states, since it smears out the line over an energy interval given by the energy dispersion of the Bloch band.

Since both effects are closely related to the population distribution of the states, they will be considered in the subsequent section in more detail.

E. Population dynamics

At the crystal surface the population of a channeling state characterized by k_y and the combined index $n=(i,\kappa_i)$ by an incoming plane wave $|\vec{K}\rangle$ is usually approximated as

$$P_n(k_y, z=0) \approx |\langle \vec{K} | k_z, k_y, \kappa_i, i \rangle|^2 = \delta_{K_z,k_z} \delta_{K_y,k_y} |\langle K_x | i, \kappa_i \rangle|^2. \quad (10)$$

Here the k_z dependence of P_n can be ignored, since k_z does not change significantly during the passage of the channeling electron through the crystal; i.e., the distribution in k_z remains very sharply peaked around its initial value for channeling in the MeV region. Propagation of $P_n(k_y,z)$ in time t or equivalently in crystal depth $z=ct$ is given by a master equation, similar to that in Ref. 32,

$$\frac{d}{dz} P_n(k_y,z) = \sum_{n'} \int dk_y' W_{n,n'}(k_y - k_y') P_{n'}(k_y',z), \quad (11)$$

with a transition probability $W_{n,n'}(k_y - k_y')$ that contains a gain and a loss term,

$$W_{n,n'}(k_y - k_y') := \sum_i \left(\frac{d^3 W_{nn'}^i}{dz\,d\kappa\,dk_y} - \delta(k_y - k_y')\,\delta_{nn'} \sum_{n''} \int dk_y'' \frac{d^3 W_{n''n}^i}{dz\,d\kappa\,dk_y''} \right) \Delta\kappa. \quad (12)$$

Here $\Delta\kappa$ means the interval of the discrete Bloch momentum κ on an appropriate grid in momentum space. The sum over i runs over all mechanisms that contribute to a redistribution of population, essentially thermal and electronic scattering, while radiative transitions can be neglected.

Further simplification of the master equation (11) can be obtained by an approximative ansatz for the density of the k_y distribution,[30]

$$p_n(k_y,z) := \frac{dP_n(k_y,z)}{dk_y} = \frac{\beta_n}{\sqrt{2\pi\alpha_n}} \exp\left(-\frac{k_y^2}{2\alpha_n}\right). \quad (13)$$

Here $\alpha_n(z)$ and $\beta_n(z)$ are the depth-dependent k_y variance and total population of the nth channeling state, respectively. If we insert this ansatz into the master equation (11) and take its zeroth and second moments with respect to k_y, we find a system of coupled differential equations for α_n and β_n,

$$\frac{d}{dz}\beta_n = \sum_{n'} W_{nn'}^{(0)} \beta_{n'}, \quad (14)$$

$$\frac{d}{dz}\alpha_n = \sum_{n'} \frac{\beta_{n'}}{\beta_n} [W_{nn'}^{(2)} + (\alpha_{n'} - \alpha_n) W_{nn'}^{(0)}]. \quad (15)$$

Here the zeroth and second moments of the transition density [Eq. (12)], $W_{nn'}^{(0)}$ and $W_{nn'}^{(2)}$, have been introduced. One should note that the first equation for β_n is closed and displays the same structure as the original master equation [Eq. (11)]. Actually it coincides with the master equation given in Ref. 32 for the population of the nth level averaged over k_y. However, Eq. (15) couples the time (more precisely,

depth) evolution of α_n to that of β_n. It allows the calculation of $\alpha_n(z)$, provided that $\beta_n(z)$ is determined in a first step from Eq. (14).

F. Radiation spectrum

After solving these equations numerically the emitted channeling radiation spectrum can be calculated by multiplying Eq. (3) with (13) and integration over the crystal depth. If, furthermore, taking into account the finite lifetime of the channeling states, the δ function in (3) is substituted by a line of Lorentzian shape and finally an integration over all Bloch momenta in the first Brillouin zone is performed, one obtains the emitted number of photons per electron in the forward direction,

$$\frac{d^2N_{fi}}{d\omega d\Omega}=\frac{e^2}{\pi(mc^2)^2}\hbar\omega\int_{-g_0/2}^{g_0/2}d\kappa b\left|\left\langle f,\kappa\left|\frac{p_x}{\hbar}\right|i,\kappa\right\rangle\right|^2\int_0^L dz\,\frac{\beta_i(\kappa,z)}{\sqrt{2\pi\alpha_i(\kappa,z)}}$$
$$\times\int dk_y\exp\left(-\frac{k_y^2}{2\alpha_i(\kappa,z)}\right)\frac{1}{\pi}\,\frac{\Gamma_{fi}/2}{(\Gamma_{fi}/2)^2+\left(\hbar\omega-\dfrac{\hbar\omega_{if}}{1-\beta\cos\vartheta}\right)^2}, \tag{16}$$

where the continuous limit for the so-far discrete Bloch momentum κ has been performed for notational convenience and the densities $\beta_i(\kappa,z)$ and $\alpha_i(\kappa,z)$ were defined as

$$\beta_i(\kappa,z)=\lim_{\Delta\kappa\to 0}\frac{\beta_{(i,\kappa)}}{\Delta\kappa},\quad \alpha_i(\kappa,z)=\lim_{\Delta\kappa\to 0}\alpha_{(i,\kappa)}(z). \tag{17}$$

In Eq. (16) the y momentum k_y is related to the angle of divergence ϑ via $k_y=K\sin\vartheta$. Thus, the Doppler broadening of the spectral line $i\to f$ is seen to be dependent on the k_y variance $\alpha_i(\kappa,z)$. Similarly the Bloch wave broadening is essentially determined by the distribution $\beta_i(\kappa,z)$, since $\alpha_i(\kappa,z)$ is expected to be weakly dependent on the Bloch momentum κ.

Solutions of Eq. (1) were calculated using the well-known many-beam method,[36] i.e., a Fourier expansion of Eq. (1). There were 61 beams included and no variation of the results was found by further increasing this number. For the crystal potential two different approximations were applied. First, the crystal potential was approximated by the widely used superposition of atomic potentials, centered at the lattice sites of the crystal. For the atomic potential the numerical results of Doyle and Turner[37] were used, however, in the form of an improved fit by Burenkov *et al.*[38]

The purely atomic potential proved to be sufficient for single planes like (110), but it showed deviations from experimental results for the double planes like (111), since in this case a C-C bond lies within the double-well potential, thus affecting the screening of the Coulomb potential by the crystal electrons more strongly than in the first case, where the bond lies between the planes. For a second approximation we tried to take into account the altered screening by using a genuine crystalline valence electron density calculated in Ref. 39. It showed a better agreement of the theoretical and experimental results[30] for the (111) plane, while it did not differ significantly from the usual atomic potential for the (110) plane.

In Sec. IV the measured spectral densities are compared to our calculations. For this purpose Eq. (16) has to be summed up over final and initial states f and i, respectively. Significant contributions to the channeling lines and to the spectral background are provided by transitions between the lowest 10–15 states only. However, for the numerical solution of Eqs. (14) and (15) a sufficient number of states has to be included into the calculation, to enable the depopulation of low-lying states by scattering into higher bands. This number was estimated in Ref. 30 to be of the order of 50–100 for the thickest crystal used in our experiments (55 μm).

Besides applying the approach described above we have also calculated the linewidth following an idea proposed by Ref. 40 which is based on an optical potential approach.[32] Using the expression that connects real and imaginary parts of the potential, derived by Ref. 41, and the data for the different contributions to the scattering of the electrons according to Ref. 42 allows one to calculate the Fourier components of the potential. The results of our calculation are presented in Sec. IV.

III. EXPERIMENTAL PROCEDURE

A. Experimental setup

The experiments were performed at the low-energy channeling site immediately behind the 10 MeV injector of the 130 MeV superconducting electron linear accelerator S-DALINAC in Darmstadt. The essential features of the setup have been described earlier[19,23,25] and thus a detailed description of the layout is omitted here. It should be emphasized, however, that at the Darmstadt channeling facilities, the electron beam interacts with the radiation-producing crystal without passing through intensity-reducing and disturbing background-producing apertures. In contrast to our former experiments we have replaced the original two-axis goniometer by a three-axis device that allows crystal mapping and observation of axial and planar channeling.

For the current investigations the electron beam energy was set to be 5.2 and 9.0 MeV. The beam divergence was found to be of the order of 0.3 mrad. In order to keep the beam divergence at its minimum value the beam spot was observed at two CrO beam viewers placed 1.0 m before and

behind the crystal, then optimized, and routinely checked during the running procedure. The beam dimensions were always kept below a diameter of 1.0 mm as observed on a viewing screen placed at the crystal position.

After passing the crystal the electrons were bent by a magnet into a Faraday cup located 2.0 m behind the magnet. The current was selected to be in the range of 1 nA and the energy spread was measured to be $\triangle E/E \sim 2\times 10^{-3}$. While transpassing the crystal the electron beam dimensions are affected by the scattering of electrons inside the crystal, which results in an enlargement and a subsequent incomplete charge collection by the Faraday cup. In order to assure a proper measurement of the electron beam current, it became standard procedure to check routinely the incoming beam current by removing the crystal via remote control and to determine the ratio I/I_0 of electrons collected by the Faraday cup with and without the crystal. The intensity I was monitored constantly.

In the present work four diamond crystals of type Ia and IIa were prepared by grinding thicker samples down to the desired thickness. A precise measurement of their thicknesses (13 ± 2, 20 ± 2, 30 ± 2, and 55 ± 2 μm) was accomplished by applying several independent methods such as Fourier infrared spectroscopy, energy loss of alpha particles, bremsstrahlung production, and photon absorption.

The channeling radiation was detected under zero degrees by means of a Si(Li) detector connected directly to the vacuum system of the accelerator, which was shielded by 60 cm of lead. The distance between crystal and detector amounted to 250 cm and the solid angle to 2.6×10^{-6} sr. The solid angle and the detector efficiency were determined by several independent methods making use of the $1/E$ shape of the bremsstrahlung spectrum and applying an x-ray fluorescence technique, respectively.[19,23,25] For electrons of 5.2 and 9.0 MeV the cone of channeling radiation extends to about 5° and 3°, respectively, and thus only one and three, respectively, out of 10^4 photons produced are detected by this arrangement.

B. Experimental procedure, data acquisition, and reduction

After mapping a prealigned crystal the following procedure was applied. During one run of typically 8–10 h one crystal was studied at one energy. In general data were collected for two different planes and one axis. In each case also background spectra resulting with the crystal in random orientation, long-term spectra with high statistics, and scans consisting of the spectrum collection as a function of the tilt angle between crystal and electron beam direction were recorded. The cw character of the beam allowed us to collect up to 100 spectra within 8 h even at a beam current of only 1 nA, which was selected so low in order to avoid pileup effects that might occur in the Si(Li) detector and its subsequent electronics.

Data acquisition was achieved by means of conventional electronics located partially immediately near the detector. From the analog-to-digital converter (ADC) outside the accelerator hall the data were transmitted to the control room located 40 m away.

Some typical background subtracted spectra for planar and axial channeling are displayed in Figs. 1 and 2, respectively. In the planar case (Fig. 1) especially the radiation from the (110) plane shows one isolated line at about 8 keV for 9.0 MeV electrons, while for the (111) plane several transitions can be observed. The structure in the spectrum of the (100) plane is less pronounced and therefore these transitions are not further considered in the present paper. The axial spectrum taken at 5.2 MeV with the same crystal shows a number of transitions from 2.6 to 24.6 keV. The identification of the transitions denoted by the solid lines on top of the abscissa will be discussed below. In general it can be stated that the channeling spectra obtained from diamond crystals are of low background (compare also Fig. 1 of Ref. 20) and that at the position of the strongest line channeling radiation exceeds the background by a factor of 8.

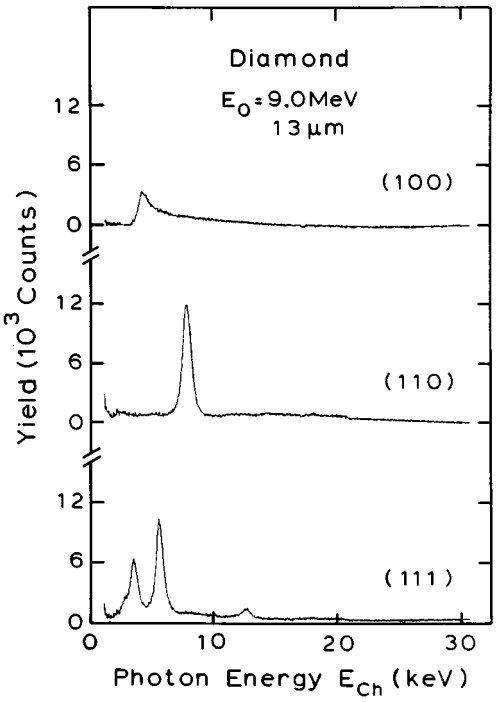

FIG. 1. Typical planar channeling radiation spectra obtained by bombarding the thinnest diamond crystal of 13 μm with 9.0 MeV electrons. The background obtained with the crystal in random orientation has been subtracted.

In order to assure a consistent reduction of the data a deduction procedure was developed that took into account background and bremsstrahlung subtraction, correction for the detector efficiency, and the self-absorption of photons inside the crystal, energy calibration, and charge normalization. The spectra were subsequently deconvoluted by fitting a Voigt function, i.e., a convolution of a Gaussian and a Lorentzian in the parametrization of Ref. 43, to the bound-to-bound transitions, a Gaussian to describe the free-to-free and free-to-bound transitions, and with -1/E-varying function to describe the contributions caused by the background with the crystal in random position, which exhibited an increasing intensity under channeling conditions which had to be taken into account. The result of such a fitting procedure is illustrated in Fig. 3.

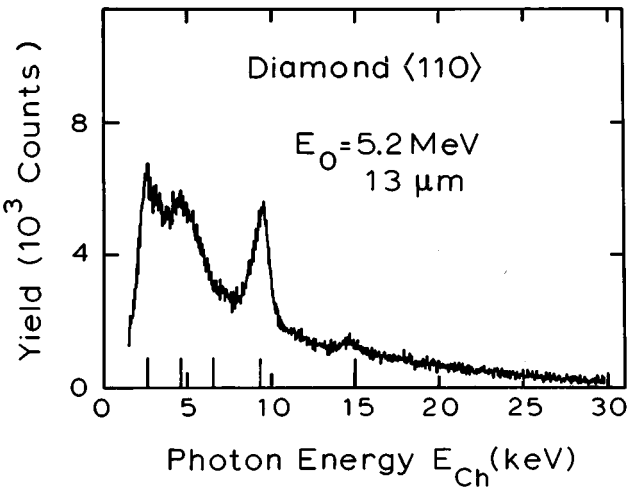

FIG. 2. Axial channeling radiation spectrum for an electron energy of 5.2 MeV. Background caused by bremsstrahlung has been subtracted. The positions of various transitions as calculated in a single-string approximation are indicated by the black bars.

IV. RESULTS AND DISCUSSION

By means of the above-described procedure the observables intensity, linewidth, and transition energy could be deduced. The data will be presented for planar and axial channeling in this section and will be compared to the theoretical predictions derived within this work. This will result in a comparison between experimental and theoretical channeling spectra and a subsequent deduction of the $1/e$ occupation length, the equipopulation length, and the coherence length.

A. Intensity and occupation length

The results obtained with respect to the intensities of the transitions[44] are listed in Table I for planar and axial channeling radiation, and are displayed partially as a function of the crystal thickness and the tilt angle in Figs. 4 and 5, respectively. The intensity as a function of electron impact energy, which confirmed the predicted $\gamma^{5/2}$ dependence, has been presented before.[20]

Inspection of the data reveals several striking features. First of all, it becomes apparent that the 1-0 transition of the (110) plane is by far the strongest. In this case only one prominent line governs the spectrum. The maximum intensity detected amounts to 0.08 photons/$e$sr achieved with the thick crystal at 9.0 MeV. In the (111) plane the 2-1 transition is the strongest. Second, for 9.0 MeV an increase of intensity with crystal thickness is observed for both transitions displayed in Fig. 4. The behavior observed at 5.2 MeV is somewhat different (lower part of Fig. 4). In this case the transition energy is of only a few keV, which causes major self-absorption of the radiation in the crystal. Third, with increasing electron energy the intensity changes dramatically according to the $\gamma^{5/2}$ dependence. In the present case the intensity of the planar radiation increases by a factor of 20 from one energy to the other. Fourth, a comparison between planar and axial intensities shows that the strongest line, i.e., the $2p$-$1s$ transition of the $\langle 110 \rangle$ axis, has about 70% of the intensity of the 1-0 transition in the planar case at 9.0 MeV. The higher axial intensity at 5.2 MeV originates from the higher transition energy in this case, which does not suffer

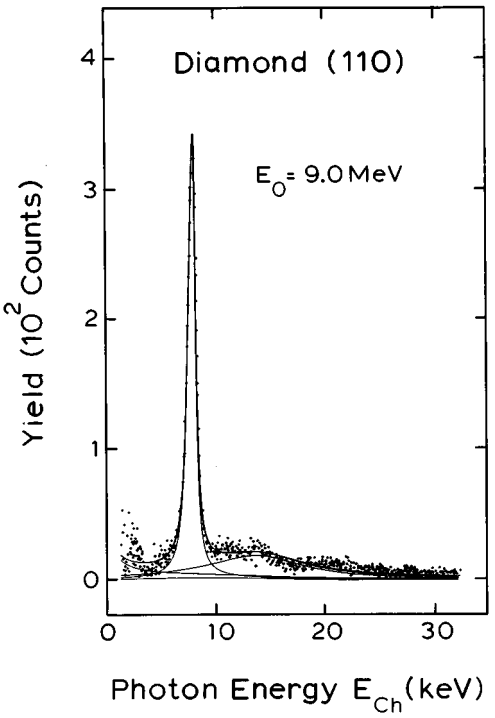

FIG. 3. Result of the fitting procedure to deconvolute the channeling spectrum of the (110) plane by means of a Voigt profile to the main transition, a Gaussian to the free-to-free and free-to-bound contribution, and with -1/E-varying function for the additional background and bremsstrahlung under channeling condition.

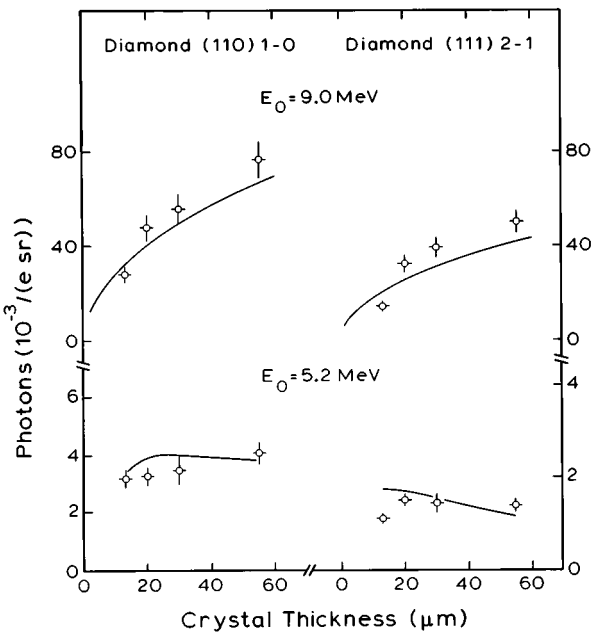

FIG. 4. Photon yield as a function of crystal thickness for two different planes and energies. The solid curves are the result of the theoretical calculation, which in the case of 5.2 MeV had to be multiplied with a factor of 0.55 for the (110) plane and 0.38 for the (111) plane. At 9.0 MeV no normalization factor was needed.

TABLE I. Number of photons/e sr in units of 10^{-3} for planar and axial channeling in diamond at 5.2 and 9.0 MeV. The values listed in roman are the experimental values, those listed in italics the theoretical values.

E_0 (MeV)	13 μm	20 μm	30 μm	55 μm
		(110) plane		
		1-0		
5.2	3.2±0.3	3.3±0.3	4.7±0.5	4.1±0.4
	6.1	*7.1*	*7.2*	*6.9*
9.0	27.8±3.2	48.4±5.7	56.1±6.4	77.0±7.9
	32.0	*42.5*	*50.0*	*65.9*
		(111) plane		
		2-1		
5.2	1.1±0.1	1.5±0.2	1.4±0.2	1.4±0.2
	4.5	*4.5*	*4.0*	*3.0*
9.0	14.9±1.6	32.9±3.8	39.5±4.9	50.9±4.9
	20.0	*25.0*	*31.3*	*41.2*
		1-0		
9.0	1.5±0.2	1.4±0.2	1.7±0.3	2.4±0.4
	2.9	*4.1*	*4.3*	*6.4*
		3-2		
9.0	9.4±1.5	13.1±2.1	23.4±2.9	25.4±4.3
	11.0	*14.6*	*17.0*	*17.3*
		4-1 and 3-0		
9.0	2.7±0.2	5.0±0.5	6.0±0.7	7.7±0.8
	3.4	*4.5*	*4.9*	*7.3*
		⟨110⟩ axis		
		2p-1s		
5.2	5.5±0.6	9.8±1.2	12.5±1.4	19.0±2.0
9.0	20.0±3.0	35.1±4.1	43.0±5.2	68.1±6.0
		3d-2p		
5.2	4.7±0.7	7.8±0.8	9.4±1.0	14.1±1.7
9.0	15.1±1.6	23.2±3.0	28.0±3.2	44.2±5.0
		3p-2s		
5.2	2.6±0.3	4.4±0.6	5.9±0.7	8.5±0.9
9.0	10.2±0.9	19.1±1.5	25.2±4.0	38.0±3.8

from absorption inside the crystal. Finally, regarding the intensity as a function of the tilt angle (Fig. 5) it can be stated that with increasing crystal thickness the distributions become broader and the relative intensity minimum at 0° less pronounced (see also Table II). The increase of intensity with the thickness is also apparent in this presentation. The larger broadening for thick crystals is caused by initially unbound electrons that are scattered into bound states with increasing probability. This effect is amplified with the crystal thickness. The decreasing intensity minimum at 0° can be explained by the same arguments. A further contribution to this effect might be due to the mosaic spread of the natural diamonds.

For planar channeling the results from the theoretical approach presented in Sec. II, Eq. (15), are listed in Table I as well, theoretical values denoted in italics, and are displayed also in Figs. 4 and 5 by solid lines. The calculations take into account the population dynamics of the states as expressed by the master equation (10) and the finite divergence of the electron beam. In case of the 9.0 MeV measurement, especially for the (110) plane, the agreement between experiment and theory is better than 11% (Fig. 4). It should be pointed out that for the theoretical description of the scattering process thermal as well as electronic scattering had to be taken into account in order to achieve the above-mentioned agreement. It turns out that for the present case of diamond the electronic scattering, although somewhat smaller than thermal scattering, is not negligible at all, which is in contrast to observations made with Si and Ni crystals.[13,18] However, electronic scattering plays a more important role for the linewidth than for the intensities.[30] To the linewidth thermal and electronic scattering contribute with equal weight. The population redistribution is in contrast dominated by thermal scattering, due to the much larger momentum transfer of this scattering mechanism. It causes scattering events into more distant energy bands and is thus more effective for depopulation. For the width only the total probability for scattering

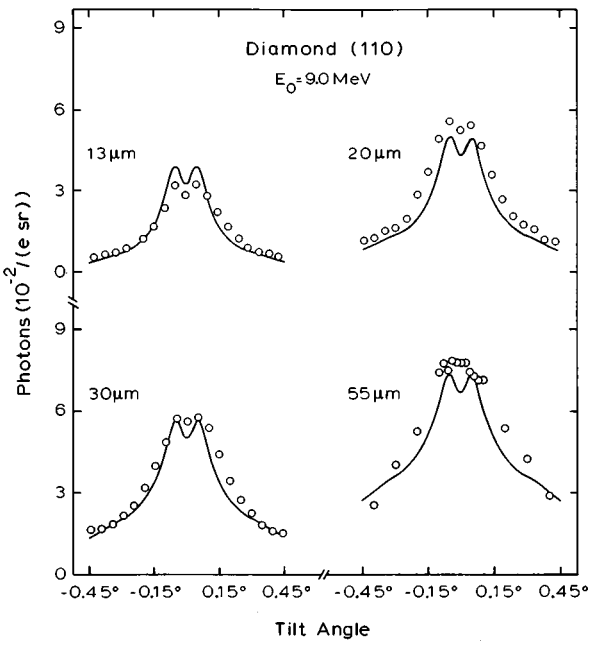

FIG. 5. Angular distribution of photon yield as function of the tilt angle for the four diamond crystals investigated. The solid lines represent the results of the theoretical calculation for each individual spectrum.

into any other band is important, regardless how far away, and thus electronic scattering contributes to the same extent as thermal.

For the 5.2 MeV data the theoretical values had to be multiplied by a factor of 0.55 for the (110) plane and 0.38 for the (111) plane in order to achieve agreement with the experimental findings. This implies that for this energy theory predicts more intensity than observed. The origin for this discrepancy is not quite clear. Evidently the scattering probabilities are larger than assumed and also lattice defects may be of more importance at lower energies. Regarding the tilt curve (Fig. 5) it can be stated that the agreement between experiment and theory is very good. Only the minimum at 0° is apparently overestimated, which indicates also that the scattering probability is underestimated or the imperfect structure of the natural diamonds is non-negligible.

The $1/e$ occupation length, which describes the distance over which the population of a state decreases by a factor of $1/e$, is intimately related to the intensity as shown before.[20] Assuming an exponential decrease of the population, which is suggested by an approximate solution of the master equation, the $1/e$ occupation length l_{occ} is obtained by fitting an expression for the intensity $I \sim 1-e^{-\lambda z}$, with $\lambda = l_{\mathrm{occ}}^{-1}$, to the data points (Fig. 4) as a function of the crystal thickness. The values deduced are combined in Table III. Inspection of the planar data yields that the occupation length increases with electron impact energy as predicted by Refs. 24,36. For constant energy the lower-lying states are characterized by a smaller occupation length than the higher states. This may be caused by the considerably stronger interaction of electrons in these states with the plane but also by an enhanced feeding of other states. In order to compare the values deduced in the current work with experimental findings[18] for Si, the Si occupation length for the (110) plane and $n=1$ was scaled according to Refs. 24,36 to an energy of 9.0 MeV, taking into account the charge of the crystal atoms, and was found to be 20 μm. This value is about 35% smaller than the planar diamond value. This can be explained since the scattering of electrons in diamond is probably much smaller than in Si crystals, since the large Debye temperature of diamond results in a smaller thermal vibration amplitude and thus a reduced scattering probability. It is interesting to note that the occupation length for axial channeling is larger. This may be caused by the fact that in planar channeling the interaction between the electrons and the plane is considerably higher than in axial channeling. On the other hand there are more bound states in the axial case, which might cause more feeding of states.

As shown in Sec. II the population of states varies as a function of the crystal thickness. The exponential decay assumed above holds only above a so-called equipopulation length l_{eq}. Below this value the population is quite different for every state and it depends on the initial population, which is a function of the electron beam divergence and the entrance angle of the beam onto the crystal, and various processes that might feed or depopulate the state. The initial population is different for even and odd states. Electron beams with divergence $\phi < 2$ mrad allow a large population of even states while odd states are populated less frequently (Fig. 6). Because of scattering processes, these populations change along the electron path through the crystal, resulting in a decreasing population of even states and an increasing

TABLE II. Width of the tilt curves obtained for planar channeling.

E_0 (MeV)	13 μm	20 μm	30 μm	55 μm
		(110) plane		
		1-0		
5.2	0.75±0.02	0.51±0.02	0.84±0.02	1.12±0.02
9.0	0.35±0.02	0.39±0.02	0.48±0.02	0.61±0.03
		(111) plane		
		2-1		
5.2	0.54±0.02	0.61±0.03		
9.0	0.30±0.03	0.33±0.02	0.40±0.02	0.54±0.02
		3-2		
9.0	0.25±0.02	0.27±0.02	0.35±0.02	0.47±0.01

TABLE III. Experimental 1/*e* occupation lengths in diamond.

E_0 (MeV)				
		(111) plane		
	1-0	2-1	3-2	4-1
5.2		18.9±2.4		
9.0	29.3±4.1	28.8±3.9	34.6±4.3	29.4±3.5
		(110) plane		
	1-0			
5.2	17.5±1.5			
9.0	27.6±3.4			
		⟨110⟩ axis		
	2*p*-1*s*	3*d*-2*p*	3*p*-2*s*	
5.2	52.4±10.1	41.0±8.5	46.1±9.3	
9.0	79.4±12.0	67.8±11.3	85.6±12.0	

population of odd states at the beginning of the path (Fig. 7). The feeding of odd states is finally compensated by losses and beyond this characteristic length, l_{eq}, each state exhibits the above-described behavior of decreasing population only. The present theoretical calculations for diamond show that the equipopulation length for the three bound states amounts to 2.2 μm at 9.0 MeV, while it is between 3.3 and 17 μm for the following unbound states denoted by $n=3$–$n=9$. These values are about one order of magnitude larger than those calculated before[36] for Ni. Finally, it becomes apparent that for the ten states considered a statistical equilibrium is observed at a depth of about 20 μm where all states attain about the same population.

B. Spectral distribution, linewidth, and coherence length

The theoretical approach outlined in Sec. II allows one to calculate the entire channeling spectrum consisting of the dominant bound-to-bound transitions, as well as the most important free-to-bound and free-to-free transitions. The theoretical intrinsic linewidth of the transitions is obtained from these calculations. The quality of the procedure can be examined from the following figures. In Figs. 8–11 the measured and calculated spectra are displayed for two planes and two energies and all crystals investigated. The theoretical calculations take into account thermal and electronic scattering, both for the occupation dynamics according to Eqs. (14) and (15) and the intrinsic linewidth and, furthermore, Bloch and Doppler broadening of states. For the initial population the finite beam divergence has been taken into account as well as the fact that the radiation intensity is modified by the self-absorption inside the crystal. A total of 15 states has been considered, which means that also free-to-bound and free-to-free states were incorporated. The agreement with the experimental spectrum is quite good for all planes at 9.0 MeV and for the 55 μm crystal at all energies.

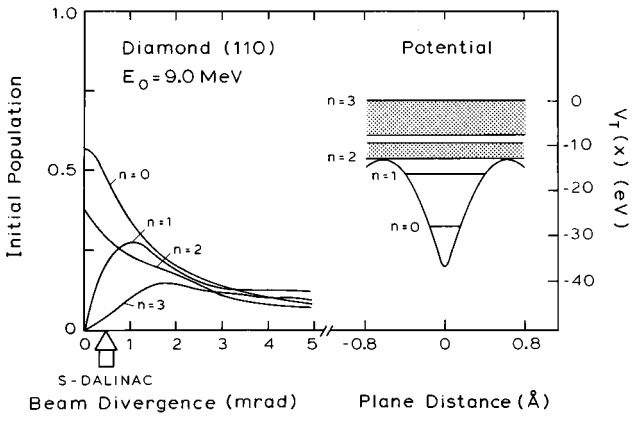

FIG. 6. Variation of the initial population as a function of the electron beam divergence (left side) and potential and the four lowest states of the (110) plane (right side). The dotted extension of the states with $n=3$ and $n=4$ represents the width of the energy band. The arrow denoted by S-DALINAC indicates the beam divergence of the present experimental conditions.

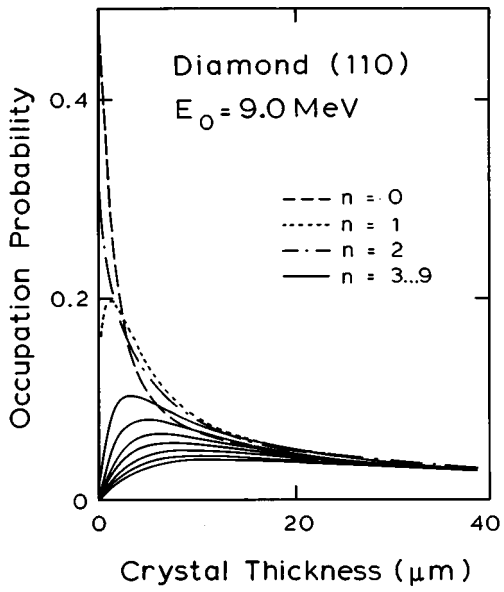

FIG. 7. Depth dependence of the population for the three bound states $n=0$, 1, and 2 and the following unbound states $n=3$–9 of the (110) plane of diamond at 9.0 MeV.

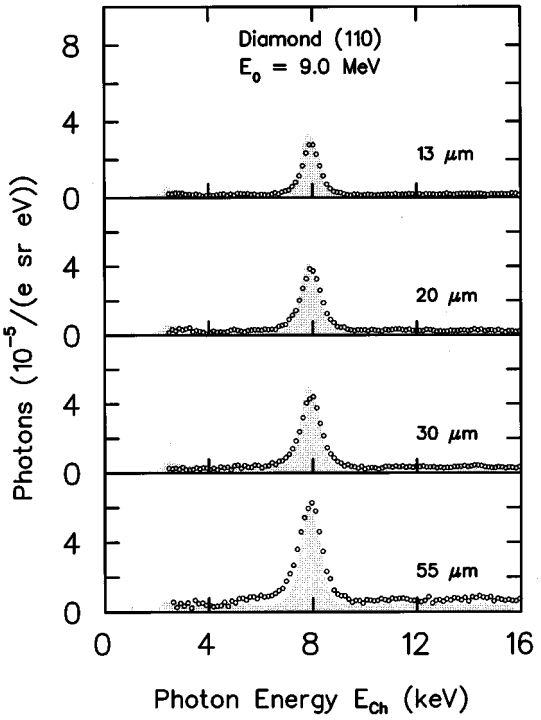

FIG. 8. Experimental points and theoretical prediction (shaded area) of the (110) planar channeling spectrum including bound-to-bound, free-to-bound, and free-to-free transitions for four different crystals at 9.0 MeV. For better representation only every fourth experimental data point has been displayed.

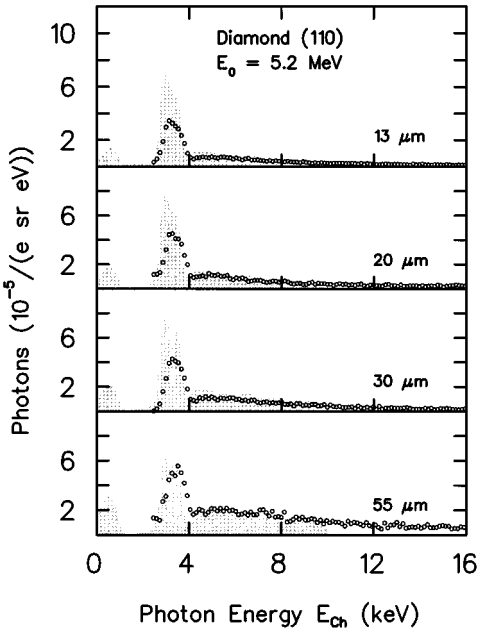

FIG. 10. Same as Fig. 8 but at 5.2 MeV.

In the first case, i.e., the (110) plane, the calculated width of the peak is too small with increasing crystal thickness, which may be explained by an underestimation of the Doppler broadening, since an additional beam divergence growth could be caused by scattering at impurities, which was not incorporated into the calculations. For the (111) plane slight deviations from the line energy are observed. This may be caused by the strong influence of the chemical bonding inside the double-well potential, which possibly could not be fully compensated for by the applied crystal potential, which was discussed in Sec. II. A further explanation could be given by the increasing background of additional bremsstrahlung, which is enhanced under channeling conditions compared to the case of a random direction. It has not been included into the theoretical calculations; nor has it been subtracted from the experiment. In the second case, where

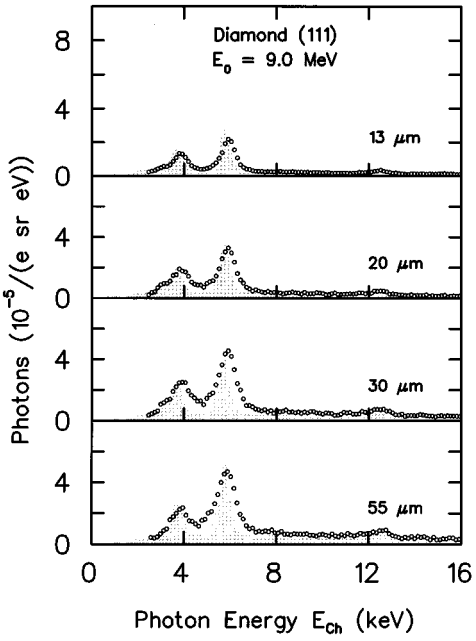

FIG. 9. Same as Fig. 8 but for the (111) plane.

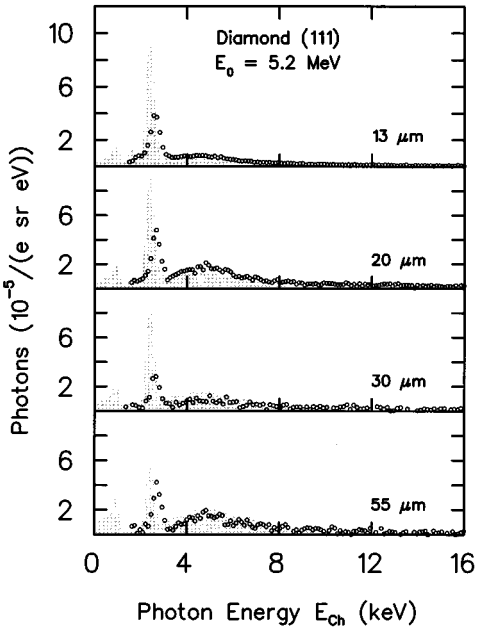

FIG. 11. Same as Fig. 9 but at 5.2 MeV.

TABLE IV. Linewidths for planar and axial channeling (roman, experimental values; italics, theoretical values).

E_0 (MeV)	13 μm	20 μm	30 μm	55 μm
		(110) plane		
		1-0		
5.2	0.79±0.02	0.86±0.02	0.86±0.02	0.98±0.02
	0.79	*0.79*	*0.79*	*0.79*
9.0	0.73±0.02	0.84±0.02	0.86±0.02	0.93±0.02
	0.66	*0.68*	*0.70*	*0.72*
		(111) plane		
		2-1		
5.2	0.24±0.04	0.29±0.06	0.36±0.06	0.39±0.04
	0.22	*0.23*	*0.23*	*0.23*
9.0	0.58±0.02	0.78±0.02	0.81±0.02	0.88±0.02
	0.41	*0.43*	*0.47*	*0.47*
		3-2		
9.0	0.69±0.03	0.97±0.03	0.95±0.07	0.52±0.03
		4-1 and 3-0		
9.0	0.98±0.08	0.77±0.08	0.72±0.10	0.80±0.20
		⟨110⟩ axis		
		2p-1s		
5.2	1.21±0.06	1.32±0.06	1.45±0.07	2.11±0.90
9.0	3.93±0.08	5.44±0.08	6.90±0.08	5.54±0.08
		3d-2p		
5.2	1.98±0.08	2.02±0.08	1.95±0.08	1.97±0.08
9.0	3.93±0.09	4.06±0.09	3.99±0.09	3.88± 0.09
		3p-2s		
5.2	0.94±0.05	1.03±0.05	1.09±0.05	1.14±0.05
9.0	3.43±0.09	3.33±0.09	3.42±0.09	3.48±0.09

satisfactory agreement was achieved, i.e., for the 55 μm crystal at all energies, the higher purity of this crystal might be responsible, being of type IIa instead of only Ia.

At low electron energies the lines show an asymmetric form, which is caused by Bloch wave broadening, whereas the Doppler broadening mainly causes the asymmetry of the lines at higher impact energies. The agreement is not as satisfactory for the three thinner crystals (13, 20, 30 μm) of type Ia at the low energy as it is at the high energy. This is not fully understood and possibly due to an energy dependence of the scattering by impurities.

The overall agreement of the planar spectral distribution can be considered as satisfactory. For axial channeling the comparison of the spectral distribution cannot be made yet. An adequate description has not been found and preliminary attempts have delivered unsatisfactory results so far.

The linewidths for the prominent transitions obtained from the experiment and the theoretical spectral distributions are listed in Table IV. Here the following features become apparent: First, the linewidth of all transitions and energies increases with crystal thickness. This is surely due to Doppler broadening described by

$$\Gamma_{\mathrm{Dop}} = 2\gamma^2 \langle \theta^2 \rangle \hbar\omega \tag{18}$$

for a radiation line with frequency $\hbar\omega$, since the mean square divergence angle $\langle \theta^2 \rangle$ increases nearly linearly with the penetration depth z. But note that Γ_{Dop} is far from being an additive or even quadratic additive contribution to the total linewidth, since the intensity of a Doppler shifted transition decreases strongly with the difference from the maximum energy. For a calculation of the contribution to the total linewidth an evaluation of Eq. (16) is unavoidable. Second, with increasing energy the linewidth stays nearly constant for the 1-0 transition of the (110) plane while it grows considerably for the 2-1 transition of the (111) plane. This effective energy independence in the (110) case is explained by two compensating effects: While the incoherent width of the ground state increases with energy the Bloch width of every bound state becomes smaller. In contrast an increase of linewidth is observed for the (111) plane since Bloch wave broadening nearly does not play any role, since the state $n=2$ in the (111) potential is more strongly bound than the state $n=1$ in the (110) and hence the 2-1 transition of the (111) is less broadened by band structure than the 1-0 for the (110). This is also expressed by the fact that the (110) plane

TABLE V. Theoretical contributions to the linewidth calculated within this work and compared with the optical potential (Ref. 42).

E_0 (MeV)	Γ_{in} (keV)	Γ_{Bloch} (keV)	Γ_{Dop} (keV)	Γ_{tot} (keV)	Γ_{opt} (keV)
		(110) plane			
		1-0			
5.2	0.09	0.72	0.15	0.79	0.16
9.0	0.18	0.56	0.35	0.72	0.37
		(111) plane			
		2-1			
5.2	0.12	0.12	0.10	0.23	0.16
9.0	0.25	0.02	0.26	0.47	0.37

has a considerable larger linewidth than the (111) plane. The comparison with theory exhibits that in general the widths are somewhat underestimated. In Table V the contributions from different broadening mechanisms as calculated according to Sec. II are shown. The incoherent linewidth Γ_{in} includes incoherent thermal and electronic scattering. The quantity Γ_{Bloch} is calculated as the difference of the minimal and maximum transition energies due to the band dispersion and Γ_{Dop} is given by Eq. (18). The total theoretical width Γ_{tot} was derived from the spectra according to Eq. (16) by determining the full width at half maximum. Furthermore, the results are compared to a very different approach to the incoherent linewidth using an optical potential method.[45,46] The latter has the disadvantage that no transition probabilities, needed for the solution of the master equation, can be obtained from it. It results in somewhat larger values for the linewidth (last column) than the perturbative approach (first column) of Sec. II. However, a decision based on our experiments in favor of one of the two methods is difficult due to the large contributions from other broadening mechanisms. It should be noted, however, that the optical potential results do not show a dependence on the chosen plane. This results from the fact that the contributions caused by thermal and core electron scattering are nearly the same for both planes since the energies of the involved transitions are very similar and since contributions from plasmon scattering are independent of the planes.

The coherence length l_{coh} is related to the intrinsic linewidth Γ_{in} according to Ref. 13 by

$$\Gamma_{in} = 2\gamma^2 \frac{\hbar c}{l_{coh}}. \tag{19}$$

From the overall agreement between the theoretical and experimental linewidth, the intrinsic linewidth that entered into the theoretical calculation was used to deduce the coherence length according to the above expression. The values obtained are listed in Table VI. It shows that the coherence length does not change with energy and that it is considerably larger for the 1-0 transition of the (110) plane. The apparent independence of the lifetime of states from the electron energy had already been reckoned before.[17] Comparing the value from Ref. 13 for Si with the diamond coherence length determined in the present work exhibits that the latter is about twice as large. This may again be explained by the lower thermal vibration amplitude in diamond. For axial channeling a coherence length can only then be deduced once a full description of all effects that contribute to the linewidth becomes available.

TABLE VI. Experimentally determined coherence length in μm for the prominent transitions in diamond.

E_0 (MeV)	(110) plane 1-0	(111) plane 2-1
5.2	0.53–0.74	0.27
9.0	0.68	0.23

C. Transition energies

In Table VII the transition energies deduced from the center of gravity of the Voigt profile fitted to the experimental spectra are listed for the planar and axial cases. The values are more or less independent of the crystal and exhibit, at least for the low-lying states, the expected $\gamma^{3/2}$ energy dependence. From the spectral distributions calculated as described above the theoretical planar values, in italics, are listed as well. For the axial transitions values calculated in a single-string approximation are listed. The agreement between experiment and theory is good for both cases.

V. CONCLUSIONS

It could be shown that the exceptional properties of the S-DALINAC electron beam enable systematic studies regarding the electron crystal interaction more efficiently than before. Due to the cw beam, data of sufficient high statistics can be collected within a few minutes.

Regarding planar channeling of diamond the investigations of the present work have been conducted in an energy region unattended so far. The strong and in the case of the (110) plane single transition exhibits intensities of up to nearly 10^{-1} photons/e sr, which suggests that the required value of 10^{12} photons/s should easily be obtained in this energy region and with moderate electron beam currents. The fairly large occupation length observed

TABLE VII. Transition energies for planar and axial channeling in keV (roman, experimental values; italics, theoretical values.

E_0 (MeV)	13 μm	20 μm	30 μm	55 μm
		(110) plane		
		1-0		
5.2	3.35±0.05	3.41±0.05	3.42±0.05	3.45±0.05
	3.27	*3.21*	*3.18*	*3.20*
9.0	7.93±0.08	7.91±0.08	7.80±0.08	7.90±0.08
	7.90	*7.90*	*7.88*	*7.9*
		(111) plane		
		2-1		
5.2	2.69±0.05	2.72±0.05	2.73±0.05	2.77±0.05
	2.39	*2.41*	*2.39*	*2.40*
9.0	5.94±0.07	5.91±0.07	5.89±0.07	5.66±0.07
	5.76	*5.72*	*5.73*	*5.73*
		1-0		
9.0	3.16±0.04	3.14±0.03	3.15±0.04	3.08±0.04
	2.91	*2.91*	*2.92*	*3.02*
		3-2		
9.0	3.84±0.04	3.82±0.04	3.85±0.05	3.80±0.05
	3.84	*3.82*	*3.85*	*3.65*
		4-1 and 3-0		
9.0	12.37±0.09	12.30±0.08	12.58±0.08	12.52±0.09
	12.34	*12.33*	*12.32*	*12.32*
		⟨110⟩ axis		
		2p-1s		
5.2	9.38±0.09	9.39±0.08	9.64±0.09	9.48±0.09
	9.32	*9.32*	*9.32*	*9.23*
9.0	24.34±0.23	2.57±0.28	24.72±0.23	24.59±0.23
	24.80	*24.80*	*24.80*	*24.80*
		3d-2p		
5.2	4.67±0.05	4.46±0.05	4.91±0.05	4.61±0.05
	4.68	*4.68*	*4.68*	*4.68*
9.0	14.56±0.15	14.51±0.15	14.76±0.15	14.55±0.15
	14.40	*14.40*	*14.40*	*14.40*
		3p-2s		
5.2	2.59±0.03	2.47±0.04	2.79±0.03	2.63±0.03
	2.63	*2.63*	*2.63*	*2.63*
9.0	8.14±0.09	7.92±0.08	8.01±0.08	8.01±0.09
	8.20	*8.20*	*8.20*	*8.20*

in diamond results presumably from a reduced scattering probability. The theoretical approach that takes into account electronic scattering besides thermal scattering describes the experimental data quite well. A scaling law predicted for the occupation length could be tested. It exhibits, however, probably crystal-specific deviations.

A comparison with results achieved lately with ruby crystals suggests that the diamond investigations should be extended to synthetic diamond crystals. In this case, the lower defect content may yield a larger occupation length and thus even higher intensities.

ACKNOWLEDGMENTS

We thank M. Reback, Johannesburg, for producing the thin diamonds and Dr. H.-D. Gräf and his crew at the S-DALINAC for providing excellent electron beams. This work has been supported by the BMBF under Contracts Nos. 06 DA 665 I, 06 BN 612 I, 06 ER 747. One of us (H.G.) acknowledges support of the FRD, Pretoria, during a visit at the University of the Witwatersrand.

[1] M.A. Kumakhov, Phys. Lett. **57**, 17 (1976).
[2] J.U. Andersen, S.K. Andersen, and W.M. Augustyniak, Vidensk. Selsk. Mat. Fys. Medd. **39**, 10 (1977).
[3] R.W. Terhune and R.H. Pantell, Appl. Phys. Lett. **30**, 265 (1977).
[4] V.G. Baryshevsky and I.Ya. Dubovskaya, Phys. Status Solidi B **82**, 403 (1977).
[5] M.J. Alguard, R.L. Swent, R.H. Pantell, B.L. Berman, S.D. Bloom, and S. Datz, Phys. Rev. Lett. **42**, 1148 (1979).
[6] R.L. Swent, R.H. Pantell, M.J. Alguard, B.L. Berman, S.D. Bloom, and S. Datz, Phys. Rev. Lett. **43**, 1723 (1979).
[7] A.O. Aganyants, Yu.A. Vartanov, G.A. Vartapetyan, M.A. Kumakhov, Chr. Trikalinos, and V.Ya. Yaralov, JETP Lett. **29**, 505 (1979).
[8] J.U. Andersen and E. Lægsgaard, Phys. Rev. Lett. **44**, 1079 (1980).
[9] J.U. Andersen, K.R. Eriksen, and E. Lægsgaard, Phys. Scr. **24**, 588 (1981).
[10] J.U. Andersen, S. Datz, E. Lægsgaard, J.P.F. Sellschop, and A.H. Sørensen, Phys. Rev. Lett. **49**, 215 (1982).
[11] V.V. Beloshitsky and F.F. Komarov, Phys. Rep. **93**, 117 (1982).
[12] M. Gouanère, D. Sillou, M. Spighel, N. Cue, M.J. Gaillard, R.G. Kirsch, J.-C. Poizat, J. Remillieux, B.L. Berman, P. Catillon, L. Roussel, and G.M. Temmer, Nucl. Instrum. Methods **194**, 225 (1982).
[13] J.U. Andersen, E. Bonderup, and R.H. Pantell, Annu. Rev. Nucl. Sci. **33**, 453 (1983).
[14] Y.H. Otsuki, Nucl. Intrum. Methods Phys. Res. Sect. B **2**, 80 (1984).
[15] R.K. Klein, J.O. Kephart, R.H. Pantell, H. Park, B.L. Berman, R.L. Swent, S. Datz, and R.W. Fearick, Phys. Rev. B **31**, 68 (1985).
[16] J.C. Kimball and N. Cue, Phys. Rep. **125**, 70 (1985).
[17] M. Gouanère, D. Sillou, M. Spighel, N. Cue, M.J. Gaillard, R.G. Kirsch, J.-C. Poizat, J. Remillieux, B.L. Berman, P. Catillon, L. Roussel, and G.M. Temmer, Phys. Rev. B **38**, 4352 (1988).
[18] J.O. Kephart, R.H. Pantell, B.L. Berman, S. Datz, and H. Park, Phys. Rev. B **40**, 4249 (1989).
[19] W. Lotz, H. Genz, P. Hoffmann, U. Nething, A. Richter, A. Weickenmeier, H. Kohl, W. Knüpfer, and J.P.F. Sellschop, Nucl. Intrum. Methods Phys. Res. Sect. B **48**, 256 (1990).
[20] U. Nething, M. Galemann, H. Genz, P. Hoffmann-Stascheck, J. Hormes, A. Richter, and J.P.F. Sellschop, Phys. Rev. Lett. **72**, 2411 (1994).
[21] R.H. Pantell, R.L. Swent, S. Datz, M.J. Alguard, B.L. Berman, and S.D. Bloom, IEEE Trans. Nucl. Sci. **NS-82**, 1152 (1981).
[22] A.C. Thompson, R. Hofstadter, J.N. Otis, H.D. Zeman, R.S. Kernoff, E. Rubinstein, J.C. Giacomini, H.J. Gordon, G.S. Brown, and W. Thomlinson, Nucl. Instrum. Methods Phys. Res. Sect. A **266**, 252 (1988).
[23] H. Genz, H.-D. Gräf, P. Hoffmann, W. Lotz, U. Nething, A. Richter, H. Kohl, A. Weickenmeier, W. Knüpfer, and J.P.F. Sellschop, Appl. Phys. Lett. **57**, 2956 (1990).
[24] C.K. Gary, R.H. Pantell, M. Özcan, M.A. Piestrup, and D.G. Boyers, J. Appl. Phys. **70**, 2995 (1991).
[25] A. Richter, Mater. Sci. Eng. B **11**, 139 (1992).
[26] K. Chouffani, H. Überall, R. Dougherty, H. Genz, P. Hoffmann-Stascheck, U. Nething, and A. Richter, Nucl. Instrum. Methods Phys. Res. Sect. B **90**, 133 (1994).
[27] E. Diedrich, G. Buschhorn, W. Kufner, M. Rzepka, H. Genz, H.-D. Gräf, P. Hoffmann-Stascheck, and A. Richter, Phys. Lett. A **178**, 331 (1993).
[28] G. Buschhorn, R. Kotthaus, W. Kufner, W. Rössl, M. Rzepka, K.H. Schmitt, H. Genz, H.-D. Gräf, P. Hoffmann-Stascheck, U. Nething, M. Lohmann, B. Reime, and L. Schildwächter, Nucl. Instrum. Methods Phys. Res. Sect. A **349**, 578 (1994).
[29] H. Genz, Nucl. Instrum. Methods Phys. Res. Sect. B **87**, 82 (1994).
[30] M. Weber, Ph.D. thesis, University of Erlangen, 1995.
[31] J. Lindhard, K. Dan. Vidensk. Selsk. Mat. Fys. Medd. **34**, 1 (1965).
[32] J.U. Andersen, E. Bonderup, E. Lægsgaard, and A.H. Sørensen, Phys. Scr. **28**, 308 (1983).
[33] M.A. Kumakhov and R. Wedell, Phys. Status Solidi B **84**, 581 (1977).
[34] V.A. Bazylev and V.V. Goloviznin, Radiat. Eff. **60**, 101 (1982).
[35] V.A. Bazylev, V.I. Glebov, and V.V. Goloviznin, Sov. Phys. JETP **64**, 14 (1986).
[36] J.U. Andersen, in *Coherent Radiation Sources*, edited by A.W. Sáenz and H. Überall (Springer, Heidelberg, 1985).
[37] P.A. Doyle and P.S. Turner, Acta Crystallogr. A **24**, 390 (1968).
[38] A.F. Burenkov, Yu.I. Dudchik, and F.F. Komarov, Radiat. Eff. **83**, 241 (1984).
[39] P.J.H. Denteneer and W. van Haeringen, J. Phys. C **18**, 4127 (1985).
[40] K. Komaki, F. Fujimoto, and A. Ootuka, Nucl. Instrum. Methods **194**, 243 (1982).
[41] C.J. Humphreys and P.B. Hirsch, Philos. Mag. **48**, 115 (1968).
[42] G. Radi, Acta Crystallogr. A **26**, 41 (1970).
[43] A.K. Hui, B.H. Armstrong, and A.A. Wray, J. Spectrosc. Radiat. Transfer **19**, 509 (1978).
[44] U. Nething, Ph.D. thesis, Technische Hochschule Darmstadt, 1994.
[45] M. Höfer, Ph.D. thesis, University of Bonn, 1994.
[46] H. Nitta, Radiat. Eff. **393**, 122 (1991).